ACS EARTH AND SPACE CHEMISTRY

http://pubs.acs.org/journal/aesccq

Article

Nitrate Reactivity in Iron (Oxy)hydroxide Systems: Effect of pH, Iron Redox State, and Phosphate

Eduardo Martinez,* Laura E. Rodriguez, Rachel Y. Sheppard, Yi Zhang, Clément A. Cid, Arezoo Khodayari, and Laura M. Barge*

Cite This: *ACS Earth Space Chem.* 2023, 7, 2287−2297

Read Online

ACCESS | Metrics & More | Article Recommendations | Supporting Information

ABSTRACT: Nitrate and phosphate are major components of fertilizers, which upon runoff can lead to the eutrophication of aqueous systems. Iron (oxy)hydroxides present a potential method for removing nutrients via denitrification/adsorption. However, the efficiency by which these contaminants are removed may be impacted by the competitive effects of compounds present in the system. Herein, we conducted anoxic experiments testing the interactions between nitrate (NO_3^-) and Fe minerals at different pH values, Fe redox state, and with the presence of phosphate (HPO_4^{2-}). In our anoxic and alkaline experiments containing 100% Fe^{2+}, approximately 20% of the initial NO_3^- concentration was reduced, while ∼60 to 80% of Fe(II)-hydroxides were oxidized. The reduction of NO_3^- and the oxidation of Fe(II) precipitates formed NH_3/NH_4^+ and magnetite (Fe_3O_4). Nitrate reduction was not observed under conditions with 100% Fe^{2+} at 6.5 or in experiments containing either 1:1 Fe^{2+}:Fe^{3+} or 100% Fe^{3+} at any pH. Upon addition of HPO_4^{2-}, nitrate reduction was inhibited, and no redox was observed. Additionally, NO_3^- inhibited HPO_4^{2-} adsorption with ferrous iron-containing minerals, although HPO_4^{2-} adsorption was observed in 100% Fe^{3+} experiments. This work demonstrates the challenges with developing treatment mechanisms for nutrient-impacted sites and elucidates how nutrients could further react with Fe (oxy)hydroxides in sediments, should they remain in the system.

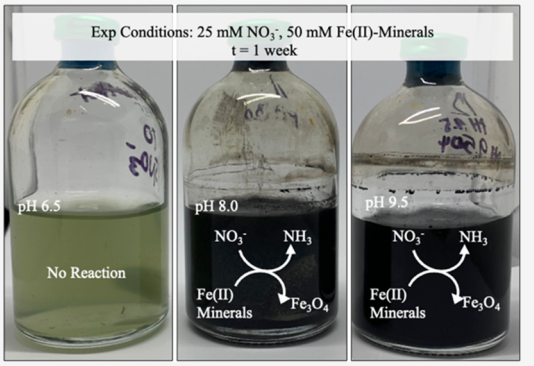

KEYWORDS: *iron hydroxides, nitrogen, phosphorus, magnetite, redox reaction, adsorption*

INTRODUCTION

Nitrogen and phosphorus are key biogenic elements that are limiting nutrients for biological growth. Understanding the role of iron (Fe) mineral systems in abiotic nitrogen (N) and phosphorus (P) cycling is key to determining the fluxes between N and P reservoirs. Nitrate (NO_3^-) and phosphate are water-soluble and ubiquitous throughout the Earth's surface and groundwater systems; they are major components of fertilizers,[1,2] and they are considered pollutants of concern from an environmental science perspective.[3] The interactions between NO_3^- and Fe have implications for environmental science; for example, in the water treatment industry, NO_3^- is considered a contaminant with a maximum contaminant level (MCL) of 10 mg/L of N, and denitrification catalyzed by Fe is regarded as an attractive method of treatment.[3]

Compared to phosphate, nitrate cycling is more complex given the various species to which nitrate can be converted, including soluble nitrite, gases that remove N from the system (N_2, N_2O), and soluble ammonia. Redox-active Fe minerals present in the subsurface oxic/anoxic transition zone can affect NO_3^- reactivity and transport through redox reactions and sorption (physical and chemical bonding, ion exchange, and absorption) depending on geochemical and/or experimental conditions.[4−10] For example, abiotic NO_3^- reduction by Fe^{2+} and/or Fe(II)-bearing minerals has been shown at elevated temperatures, at various pH levels, and/or in the presence of catalysts (Cu^{2+}, Ag^{2+}, Fe(0)).[5,10−15] The products from these NO_3^- reduction reactions include N gases (e.g., N_2O) and reduced soluble N species (i.e., NH_3/NH_4^+) as well as oxidized Fe in the form of magnetite.[11,15] Under ferric (Fe(III)-only) mineral conditions, NO_3^- and Fe(III)-(oxy)hydroxides do not undergo redox chemistry; rather, the minerals provide binding sites for the surface complexation of NO_3^-. Computational studies have shown that NO_3^- complexation can occur on Fe(III)-(oxy)hydroxides under acidic, neutral, and alkaline conditions, demonstrating that NO_3^- adsorption occurs by inner (chemical bonds) and outer (electrostatic) sphere complexes depending on the pH.[16]

However, more experimental study is needed to understand how NO_3^- interacts with Fe-mineral surfaces and how this is affected by environmental factors such as pH, iron redox state,

Received: July 20, 2023
Revised: September 29, 2023
Accepted: October 9, 2023
Published: October 26, 2023

or the presence of other competing anions (such as HPO_4^{2-}) in the system. In this work, we revisited the $NO_3^- - Fe^{2+}$ redox couple to understand the amount of NO_3^- removed from aqueous experiments by either redox reactions with or adsorption onto Fe (oxy)hydroxide minerals. The objectives of this study were to (1) quantify the magnitude of nitrate reduction/adsorption on iron minerals under anoxic conditions at circum-neutral (6.5) and alkaline (8.0 and 9.5) pH; (2) quantify ammonia production by colorimetry; (3) determine the effect of equimolar HPO_4^{2-} concentration on NO_3^- reduction and/or adsorption on Fe (oxy)hydroxides, and (4) characterize mineralogical changes in Fe oxyhydroxides due to interactions with NO_3^- in mineral systems.

METHODOLOGY

Nitrate and Phosphate Batch Experiments Using Fe (Oxy)hydroxides. All experiments were performed at ambient temperature and pressure; solutions were prepared in 100 mL serum vials sealed with black rubber butyl stoppers, crimped with aluminum crimp seals, and continuously stirred (100 rpm) on a stir plate inside a N_2-filled glovebox (Plas Labs 818 series). $FeCl_2{\cdot}4H_2O$ (Sigma-Aldrich) and $FeCl_3{\cdot}6H_2O$ (Sigma-Aldrich) were dissolved in 85 mL of Milli-Q water (18.2MΩ·cm) sparged with N_2 gas for a total Fe concentration of 250 mM. Our N_2 sparging technique is not expected to be a source of NH_3/NH_4^+ via N_2 (g) reduction;[17] in previous experiments that employed a similar experimental procedure, NH_3/NH_4^+ was not detected in any experiments sparged with N_2 (g).[18] 15 mL of 5 M NaOH was added to precipitate Fe minerals. The mineral precipitate was immediately centrifuged, and 40 mL of the supernatant was removed and replaced with Milli-Q water; this was done to remove excess Cl^- and Na^+ ions from the supernatant. Depending on the experimental condition, the pH of the Fe (oxy)hydroxide was titrated to 9.5, 8.0, or 6.5 using HCl. When the desired pH was reached, the vial was agitated to evenly mix solid and liquid, and 20 mL of the Fe (oxy)hydroxide slurry was transferred into another 100 mL serum vial and then mixed with 80 mL of a 31.25 mM $Na^{15}NO_3$ (Sigma-Aldrich) solution (that had been titrated to the same pH). This resulted in a final experimental concentration of 25 mM NO_3^- and 50 mM total Fe. A detailed list of experimental conditions can be found in Table S1.

Additional nitrate + phosphate experiments were performed to determine whether phosphate competed with nitrate for reactive sites on the Fe (oxy)hydroxide surface (Table S1). The nitrate + phosphate experiments were prepared in the same manner as above, except that 20 mL of Fe-mineral suspension was mixed with 80 mL of solution containing both nitrate ($Na^{15}NO_3$) and phosphate ($Na_2HPO_4{\cdot}H_2O$, Mallinckrodt). Both NO_3^- and HPO_4^{2-} were added, such that the total concentration of each was 25 mM in the 100 mL vial. The nitrate + phosphate experiments were only performed at pH 9.5 because this was one of the two conditions where we observed notable NO_3^- reduction in the nitrate-only experiments. In this work, we refer to hydrogen phosphate (HPO_4^{2-}) as phosphate, given that phosphoric acid speciation at pH 9.5 results in this dominant ionic form.

Control experiments were also performed using the same procedure but without nitrate or phosphate added. The controls were allowed to react for 1 week to ensure the reactions were a result of the compounds added (e.g., NO_3^- and HPO_4^{2-}). The controls were made using the same procedure as the nitrate-only experiments except with 80 mL of pure Milli-Q water (e.g., no NO_3^- and/or HPO_4^{2-} was present in the control experiments).

Sampling. Experiments were sampled six times at each time point (t = 0, 1 day, 7 days). Vials were stirred before sampling (inside the glovebox) to ensure even distribution of solid/liquid. Three of the six 1 mL samples were immediately centrifuged to analyze the NO_3^- and/or HPO_4^{2-} concentration in the supernatant via ion chromatography (IC), while the other three samples were treated with 0.5 mL of 2.5 mM HCl to dissolve the solids for colorimetry. The post-treatment of the samples was performed outside of the glovebox, and the resulting samples for analysis were stored inside a −20 °C freezer. After the final samples were taken at t = 7 days, the reaction mixture was allowed to settle and the supernatant was removed, and the mineral precipitate was subjected to lyophilization over 3 days (with a SP Scientific Virtis AdVantage Benchtop Freeze-Dryer). The freeze-dried precipitates were stored in the N_2-filled glovebox until analysis.

Ion Chromatography. Three samples from each time point were analyzed with IC. 0.75 mL of the supernatant was transferred to a new tube and treated with 0.25 M of 1 M NaOH to precipitate any remaining dissolved Fe^{2+}. The sample was centrifuged, sampled, and treated again with the same process (0.25 mL of NaOH + 0.75 mL of supernatant); this process was done a total of three times to remove residual Fe^{2+}. Then, the samples were filtered with a 0.2 μm syringe filter, diluted to 5 mL using deionized Milli-Q water, and dispensed into polyvials that were loaded onto an automated sampler. Concentrations of NO_3^-, HPO_4^{2-}, and Cl^- were measured using an Interion HPLC System fitted with a Dionex IonPac AG11-HC-4 μm column (4 mm × 250 mm). The instrument used a EGC 500 KOH eluent generator set to 30 mM concentration. Two instrument methods were created using an isocratic flow of 1.25 mL/min for a retention time of 15 min and constant current. The first IC method was used to measure NO_3^-, NO_2^-, and Cl^- of the nitrate-only experiments; in this method, the retention times of Cl^- and nitrate were 3.64 ± 0.03 and 6.78 ± 0.09 min, respectively. The second IC method was used to determine the concentrations of Cl^-, NO_3^-, and HPO_4^{2-} of the nitrate−phosphate experiments; in this method, the retention times were 3.66 ± 0.08, 6.62 ± 0.12, and 9.82 ± 0.12 min, respectively. Calibration curves were established for each of the anions tested (Figure S1). Nitrite (NO_2^-) was not measured because the Cl^- peak appeared immediately before NO_2^- and interfered with quantification.

NH_3 and Fe Colorimetry. For experiments where we observed significant NO_3^-−Fe^{2+} reactivity (i.e., 100% Fe at pH ≥ 8), two separate experiments (25 mM NO_3^- + 50 mM Fe(II) at pH 8.0 and 9.5) were preformed to investigate any ammonia/ammonium (NH_3/NH_4^+) formation. We analyzed NH_3/NH_4^+ using a colorimetric technique[19] that determines concentrations of ammonia (NH_3) in solutions at a pH of ∼11. The experiments performed for ammonium colorimetry were sampled in 1 mL triplicates at t = 0, t = 1 day, and t = 7 days. The samples for NH_3/NH_4^+ analysis were centrifuged to separate the supernatant and solids. The supernatant (0.75 mL) was treated with 0.25 mL of 1 mM NaOH to remove the dissolved Fe^{2+} and centrifuged to ensure that there was no Fe interference. 0.75 mL of the newly treated sample was treated with 0.25 mL of 1.25 mM sulfuric acid. Absorbance at a wavelength of 628 nm was used for quantification and was measured using a UV−vis spectrophotometer (Thermo

https://doi.org/10.1021/acsearthspacechem.3c00218
ACS Earth Space Chem. 2023, 7, 2287−2297

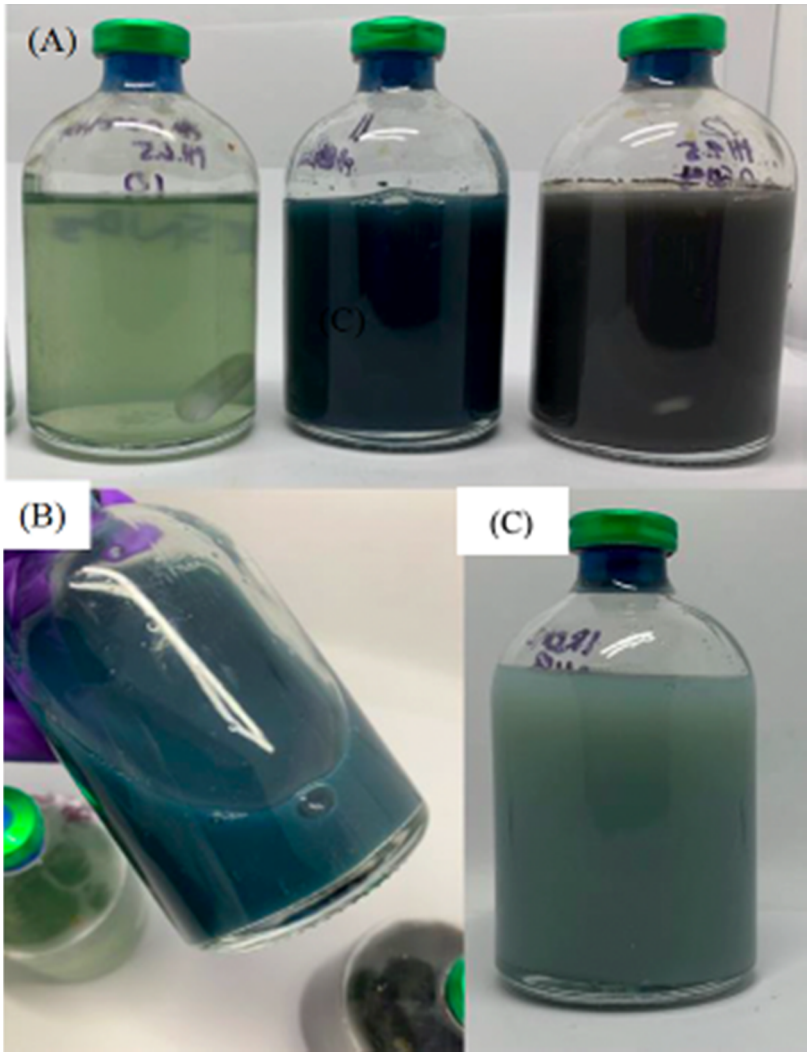

Figure 1. (A) Experimental vials containing 25 mM nitrate and 50 mM 100% Fe^{2+} after 24 h at varying pH values (left: pH 6.5, middle: pH 8.0, and right: pH 9.5). (B) Experiment with 25 mM nitrate and 50 mM 100% Fe^{2+} at pH 8.0 at 24 h. (C) Control containing only 50 mM 100% Fe^{2+} after 24 h.

Scientific Nanodrop 2000c) and a 1 cm quartz cuvette (Range: 0.62−1.35 ug/mL). The calibration curve used for the analysis can be found in Figure S2.

For Fe colorimetry, 0.5 mL of 2.5 mM HCl was added to the 1 mL sample to dissolve any solid Fe. The iron redox state was determined by using a Genesis UV−vis Spectrophotometer at a wavelength of 510 nm. The method employed measures Fe^{2+} and is described by Aguirre et al., 2020 with minor volume modifications for this study.[20] Each sample was split into two: one part was analyzed for Fe^{2+} content, while the other was first subjected to ascorbic acid to reduce Fe^{3+} into Fe^{2+} to enable the determination of the total Fe concentration. The % of Fe(II) was determined by dividing the measured Fe^{2+} by the total iron (FeT). The Fe colorimetry calibration curve can be found in Figure S3.

Visible and Near-Infrared (VNIR) Spectroscopy. Reflectance spectra were collected on the freeze-dried samples by using an Analytical Spectral Devices (ASD) FieldSpec3 spectroradiometer spanning 0.35−2.5 μm. The samples were illuminated with a fiber optic cable with a white light source mounted on a hand-held contact probe and were collected relative to a Spectralon white reference. The samples were placed on matte black Cinefoil paper to decrease background noise, and the spectra were pressed flush against the contact probe during data collection.

X-ray Diffraction (XRD). X-ray diffraction (XRD) was performed on the freeze-dried mineral samples from the end of experiments where we observed the occurrence of redox reactions (100% Fe^{2+} at pH ≥ 8.0). The dried mineral samples were transferred from 15 mL falcon tubes to 10 mL glass vials for storage. Spectra were collected on a Rigaku SmartLab X-ray diffractometer from 5 to 80°.

RESULTS AND DISCUSSION

pH-Dependent Fe-Mineral Precipitation. The addition of NaOH to the dissolved Fe solution immediately formed Fe-mineral precipitates, which varied in color, volume of precipitates, and magnetism depending on the starting pH and the Fe^{2+}/Fe^{3+} ratio. With 100% Fe^{2+}, significant amounts of precipitate only formed when pH ≥ 8.0; at pH 6.5, precipitation was not observed but the solution turned a green-translucent hue upon the addition of NaOH (Figure 1A). The colorimetry results of Fe(II)-only solutions of each pH remained consistent at nearly ∼100% Fe^{2+}/FeT throughout

https://doi.org/10.1021/acsearthspacechem.3c00218
ACS Earth Space Chem. 2023, 7, 2287−2297

the experiment (Table S7). For experiments with 50% Fe^{2+}/50% Fe^{3+}, at all pH conditions, a black material precipitated upon addition of NaOH that was attracted to the magnetic stir bar. Fe colorimetric analysis of 50% Fe^{2+}/50% Fe^{3+} showed no changes to the Fe redox state of the mineral for 1 week. For all experiments with 100% Fe^{3+}, an orange precipitate formed, regardless of the pH.

The only visually observable changes in experiments occurred at 24 h after the addition of NO_3^- (Figure 1B−1C; similar color changes observed by Buresh and Moraghan, 1976) for experiments with 100% Fe^{2+} at pH 8.0 and 9.5. The 100% Fe^{2+} with NO_3^- experiments (pH ≥ 8) reached a final color change (black magnetic particles) at 1 week where the material formed magnetic rod-shaped fragments that were attracted to the magnetic stir bar. The rods appeared similar in nature to the magnetite structures synthesized by coprecipitation methods.[21] The experiment with 100% Fe^{2+} with NO_3^- at pH 6.5 did not exhibit any color change after 1 week. For experiments with 50% Fe^{2+}/50% Fe^{3+} and 100% Fe^{3+} with NO_3^- at all pH values, no obvious changes in color or amount of precipitates were observed.

Effect of Fe-Mineral Redox State and pH on Fe/Nitrate Redox Reactions. *100% Fe^{2+} Reactions with Nitrate.* Of the conditions tested in the NO_3^--only experiments in this study, only experiments starting with 100% Fe^{2+} at alkaline pH exhibited evidence of Fe(II)-driven NO_3^-reduction. The following results only consider changes in NO_3^- concentration and the production of NH_3/NH_4^+; detection of NO_2^- was hindered by interference by Cl^- in our IC analysis and we did not have the means to detect gaseous N species (N_2, NO, and N_2O). We do recognize the possibility of NO_2^-, N_2, NO, and N_2O production that occurs in other experimental systems that contain Fe^{2+} and Fe(II) minerals at various stochiometric and experimental conditions (a summary of relevant reactions is listed in Table S2). We observed a ∼20% decrease in NO_3^- concentration (measured by IC) in the liquid phase over a period of 1 week in 100% Fe^{2+}, pH 8.0 and 9.5, NO_3^--only experiments. More specifically, by 1 week, nitrate-only experiments that started at pH 8 and 9.5 experienced a 5.32 ± 0.95 and 5.66 ± 1.32 mM decrease in NO_3^-, respectively. The decrease in NO_3^- concentration corresponds to a 20.96% ± 3.71 (pH 8) and 20.84% ± 3.89 (pH 9.5) removal percentage from experiments over 1 week (Figure 2, Table S5). This NO_3^- decrease was correlated with an increase in the average concentration of NH_3 (observed by colorimetry); specifically, the average concentrations of NH_3 increased by 1.37 mM ± 0.09 (pH 8.0) and 1.31 mM ± 0.05 (pH 9.5) (Figure 3 and Table S6) (the ± values in these results correspond to the standard deviation of technical triplicate samples of a single experiment). We also observed Fe(II) oxidation that correlated with the decrease in NO_3^- and increase in NH_3 for both pH 8.0 and 9.5 experiments (Figure 3) after 1 week, the % of Fe(II) minerals in these experiments had decreased from 92.12% Fe^{2+} to 37.84 ± 8.23% (pH 8.0) and from 91.14% Fe^{2+} to 18.76 ± 11.50% (pH 9.5) (Figure 4A and Table S8). In pH 8.0 and 9.5 experiments, we observed a drift in pH after the experiment began: for pH 8 reactions, the pH decreased on average from 8.10 ± 0.09 at t = 0 to 7.77 ± 0.25 at 1 week; for pH 9.5 reactions, the pH increased on average from 9.54 ± 0.04 at t = 0 to 11.07 ± 0.15 (Table S9). The increase and decrease in pH for the pH 8 and 9.5 reactions, respectively, despite both oxidizing Fe^{2+} and removing NO_3^- at similar rates is noteworthy. We originally

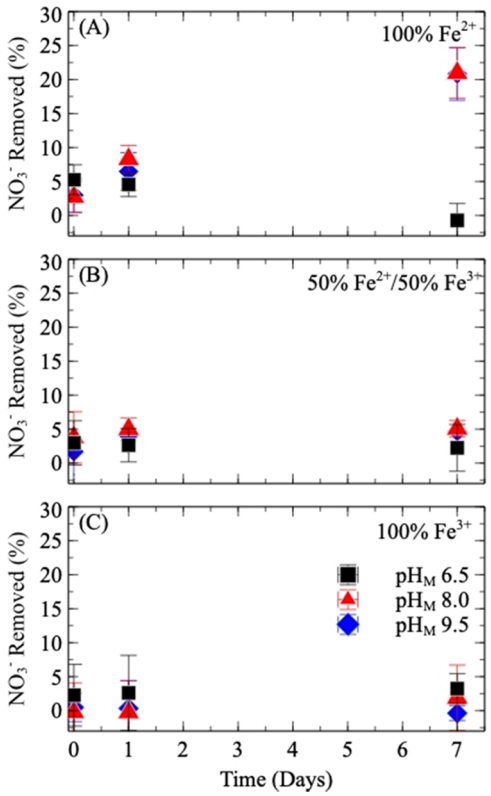

Figure 2. Average NO_3^- concentrations measured in experiments containing 25 mM NO_3^- and 50 mM Fe. (A) Experiments with 100% Fe^{2+}. (B) Experiments with 50% Fe^{2+} and 50% Fe^{3+}. (C) Experiments containing 100% Fe^{3+}. The error bars are the standard deviation of three experimental repeats.

hypothesized that the discrepancy could be due to different minerals forming at different pH values; however, VNIR showed that both reactions showed low reflectance consistent with magnetite (Figure 5A); this was further corroborated with XRD (Figure 6) that suggested magnetite was formed in both reactions (RRUFF ID: R061111.9[22]). The additional XRD peaks located at 32 and 46° likely correspond to highly crystalline halite (NaCl);[23] and in these samples, no other crystalline material was observed to be present.

In contrast, 100% Fe(II) reactions at pH 6.5 showed neither NO_3^- decrease (Figure 2A and Table S5) nor Fe(II) oxidation (Figure 4A and Table S8) over 1 week. VNIR analysis of the lyophilized solids from the pH 6.5 experiment showed absorption bands located at 1.46 and 1.98 μm that corresponded to H_2O within the mineral structure, and 0.35 and 0.85 μm absorption bands that corresponded to electronic vibrations associated with iron; this likely indicates the presence of hydrated chloride salts (Figure 5A). Finally, for the pH 6.5 reactions, the pH remained stable throughout the experiment, only increasing from 6.59 ± 0.08 (t = 0) to 6.63 ± 0.20 (1 week) (Table S9).

The differences in NO_3^- reactivity between the pH 6.5, 8.0, and 9.5 NO_3^--only experiments at 100% Fe^{2+} are likely related to the amount of Fe-mineral precipitate that was present at these conditions. The observed decrease in NO_3^- was most pronounced at high pH (8.0 and 9.5), which are also conditions that generate the most Fe-mineral precipitate mass; whereas at pH 6.5, very little mineral solid was produced (Figure 1A). At pH ≥ 8, Fe^{2+} precipitates as a mineral that provides a reactive site for surface chemistry, ion exchange, and

https://doi.org/10.1021/acsearthspacechem.3c00218
ACS Earth Space Chem. 2023, 7, 2287−2297

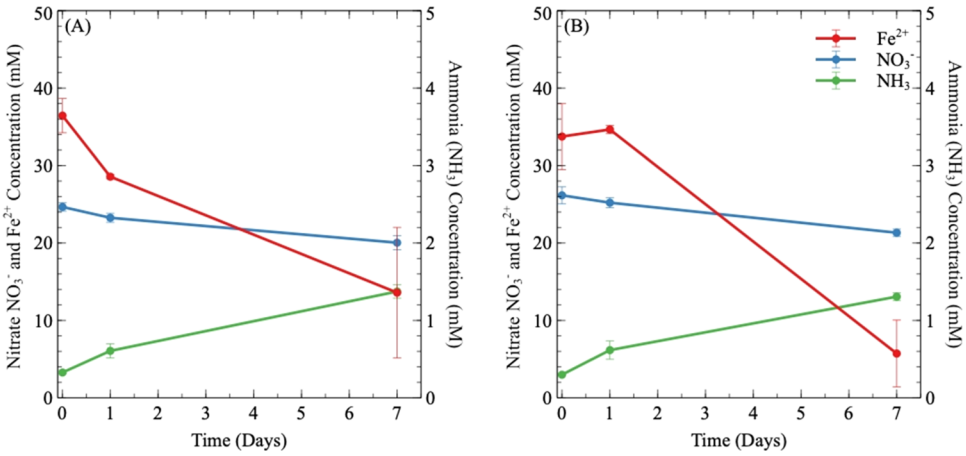

Figure 3. NO_3^-, Fe^{2+}, and NH_3 concentrations in 100% Fe^{2+} and NO_3^- experiments at alkaline pH. (A) pH 8.0. (B) pH 9.5. The error bars are the average concentration of technical triplicates.

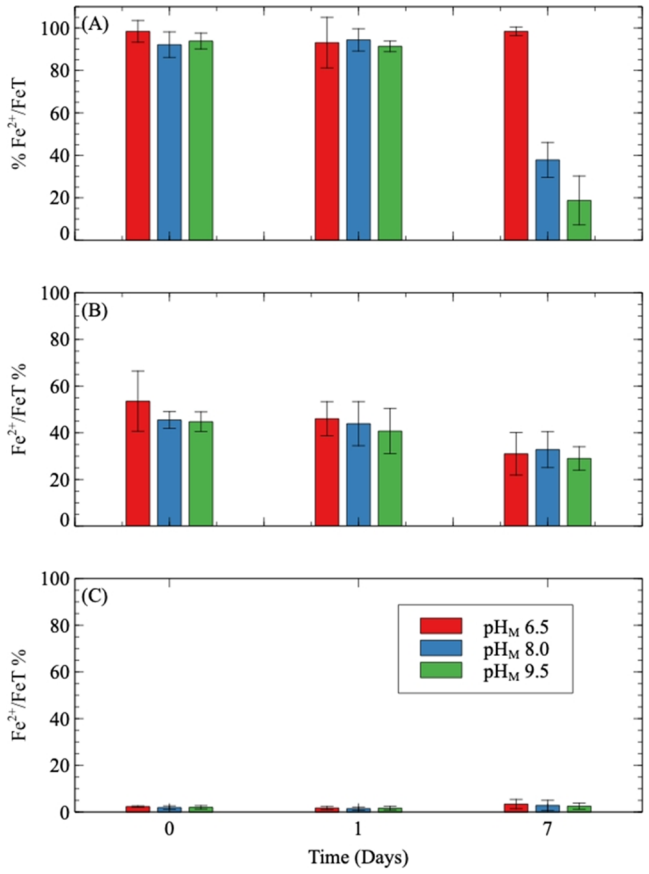

Figure 4. Oxidation of Fe^{2+} in NO_3^- -only experiments, reported as changes in % Fe^{2+}. (A) Experiments with 100% Fe^{2+}. (B) Experiments with 50% Fe^{2+}/50% Fe^{3+}. (C) Experiments with 100% Fe^{3+} (Table S8). Error bars are the standard deviation of three experimental repeats.

adsorption.[24] A previous study testing NO_3^-/Fe(II)-mineral reactions under slightly different conditions (pH 8.0, 10 mM Fe^{2+}, 1 mM NO_3^-) also observed a decrease in NO_3^- over 1 week.[11] The NO_3^--driven oxidation of Fe(II) in these iron mineral precipitates produces a black and magnetic solid likely to be magnetite (Fe_3O_4), as suggested by our results and other studies.[11,12,14,25,26] At pH 6.5, we observed neither NO_3^- reduction by nor adsorption onto Fe minerals; this could be due to the overall lack of surface sites given that a precipitate was not produced. It would seem from Figure 1A that the decrease in NO_3^- was not affected by the experimental pH, until the pH falls below a point where Fe is not sufficiently precipitated. Based on the Pourbaix diagrams by Génin et al. 2006, the precipitation of Fe^{2+} indicates E_h values in the negative range between approximately −0.55 and −0.65 V; to this end, the type of Fe species can transition between phases as a function of pH.[27]

50% Fe^{2+} and 50% Fe^{3+} Reactions with Nitrate. Experiments that started at 50% Fe^{2+}/50% Fe^{3+} experienced negligible Fe and NO_3^- reactivity. The experiments with 50% Fe^{2+} showed an approximately less than 5% NO_3^- decrease after 1 week at all pH values tested (Figure 2B and Table S5). The most notable reactivity that we observed was the slight oxidation of Fe(II) in the minerals. In a previous study, a 10% NO_3^- removal from solution was achieved using magnetite at pH 5.5.[9] Our colorimetric results indicated that the Fe(II) precipitates began to oxidize by t = 1 day and by 1 week the % Fe^{2+} decreased from 53.55% ± 12.89 to 38.55% ± 3.96 for pH 6.5, 45.50 ± 3.59 to 34.05 ± 9.83 for pH 8.0, and 44.76 ± 4.21 to 29.02 ± 5.02 for pH 9.5 (Figure 5B and Table S8). However, given that we observed no corresponding NO_3^- reduction, this slight Fe oxidation could be a result of atmospheric oxidation, while the sample was processed and analyzed outside of the anaerobic glovebox. A second notable result was that the pH of all three sets of experiments slightly decreased over 1 week (Table S9); however, this could be a result of the precipitates reaching equilibrium and not any reactions related to NO_3^- (this same pH decrease was also observed in our control experiments where NO_3^- was not present). VNIR reflectance spectra for the 50% Fe^{2+} nitrate-only experiments exhibited flat features that correspond to magnetite formation, similar to the results for 100% Fe^{2+} experiments at alkaline pH (Figure 4B).

100% Fe^{3+} Reactions with Nitrate. The NO_3^--only experiments starting with 100% Fe^{3+} showed no significant decrease in NO_3^- at any pH tested (Figure 1C); after 1 week, the NO_3^- decreased by 3.24 ± 2.21, 1.90 ± 4.82, and −0.37% ± 1.08 for the pH 6.5, 8.0, and 9.5 experiments, respectively (Figure 2C and Table S5). Fe colorimetric results showed less than ∼4% of Fe^{2+} present after 1 week which is within the experimental error; thus, no Fe redox reaction occurred with ferric minerals as expected. Lastly, the pH of the experiments

https://doi.org/10.1021/acsearthspacechem.3c00218
ACS Earth Space Chem. 2023, 7, 2287−2297

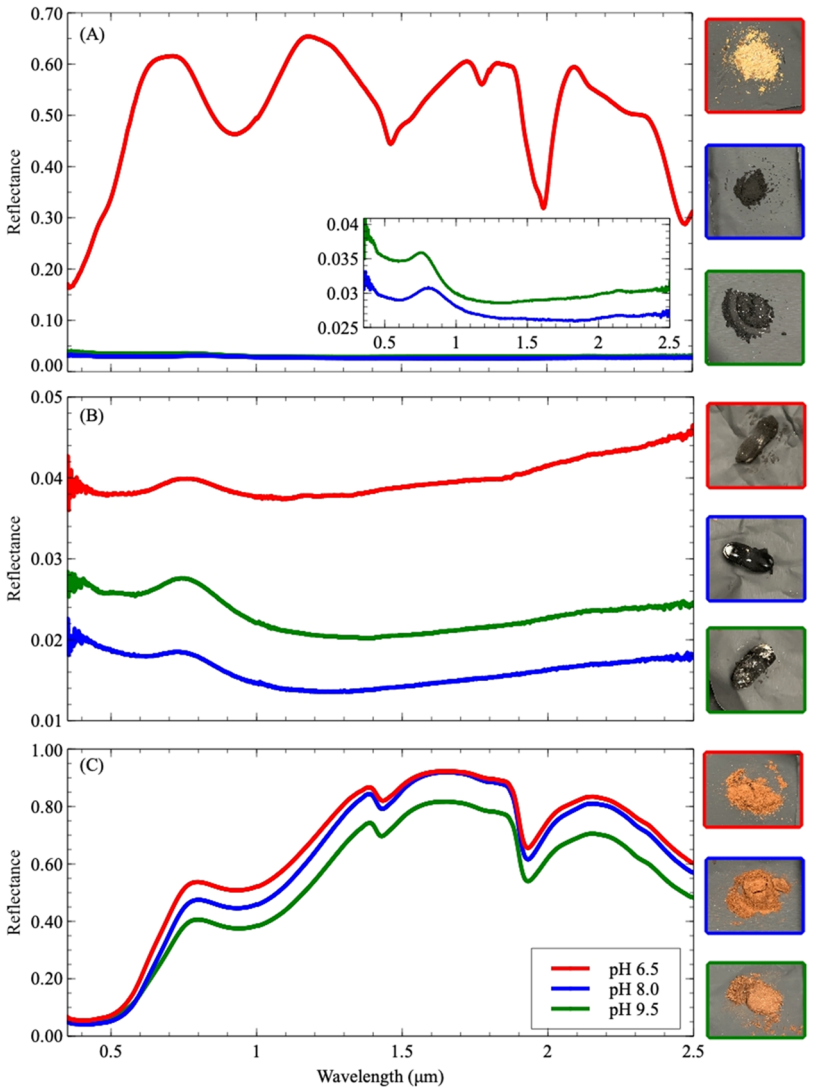

Figure 5. VNIR spectral reflectance of solid samples containing 50 mM Fe and 25 mM NO_3^- at different pH values. (A) 100% Fe^{2+}. (B) 50% Fe^{2+} and 50% Fe^{3+}. (C) 100% Fe^{3+}.

remained relatively stable (Table S9). The reflectance spectra for the Fe(III) precipitates after 1 week of reaction time with NO_3^- revealed reflectance bands similar to those of hematite (Fe_2O_3) (Figure 4C). The bands of the reflectance spectra located at 0.35 and 0.94 μm correspond to Fe−O bonds, while the bands located at 1.43 and 2.48 μm correspond to H_2O vibrations adsorbed to salts.

We would not expect Fe(II)-driven NO_3^- reduction to occur in 100% Fe^{3+} experiments; however, NO_3^- might still be removed from the liquid phase via surface adsorption to the minerals. Indeed, DFT studies have shown that NO_3^- can form ligand exchange bonds with ferric minerals under acidic, neutral, and basic conditions.[16] In laboratory experiments by Youngran et al., 2007, ∼ 2% nitrate was adsorbed onto Fe minerals at pH 6.0 in solutions containing As(V) that competed for adsorption sites.[28] The NO_3^- values we report here for experiments with 100% Fe^{3+} coincide with previous findings that imply that nitrate binds only weakly onto hematite and goethite (both ferric oxides),[8,28,29] or that Cl^- and NO_3^- anions were the least favorable ions to be adsorbed on the ferric (oxy)hydroxide minerals akageneite and goethite.[30] These results can be explained by the pK_a value of NO_3^- and the point zero charge (pzc) of hematite, the only mineral phase detected in our 100% Fe(III) nitrate-only experiments by VNIR (Figure 5C). The pzc of hematite is between pH 6.0 and 6.5;[31,32] thus, at pH 6.5, 50% of the surface of our Fe(III) precipitate would be positively charged and the other 50% would be negatively charged. For our pH 8.0 and 9.5, 100% Fe(III) precipitates, the mineral would possess a fully negatively charged surface, and thus negatively charged NO_3^- would be repelled from adsorbing. In addition, NO_3^- is a conjugate base (i.e., nitric acid is a strong acid: $HNO_3 \leftrightarrow NO_3$, p$K_a$ 1.5) and a poor electron donor; consequently, NO_3^- is not expected to readily form bonds with electron-deficient species at the mineral surface (e.g., Fe or H). Overall, the pH of our reactions favors a mineral surface that is negatively charged, which repels the NO_3^- anion, and the few locales where the mineral is positively charged are unlikely to facilitate adsorption because NO_3^- does not readily share electrons.

Effect of Phosphate on Nitrate Reactions with Fe oxyhydroxides. Given that HPO_4^{2-} and NO_3^- are common additives to fertilizers and are also critical nutrients for life, we chose to investigate systems containing both. Previous work

https://doi.org/10.1021/acsearthspacechem.3c00218
ACS Earth Space Chem. 2023, 7, 2287−2297

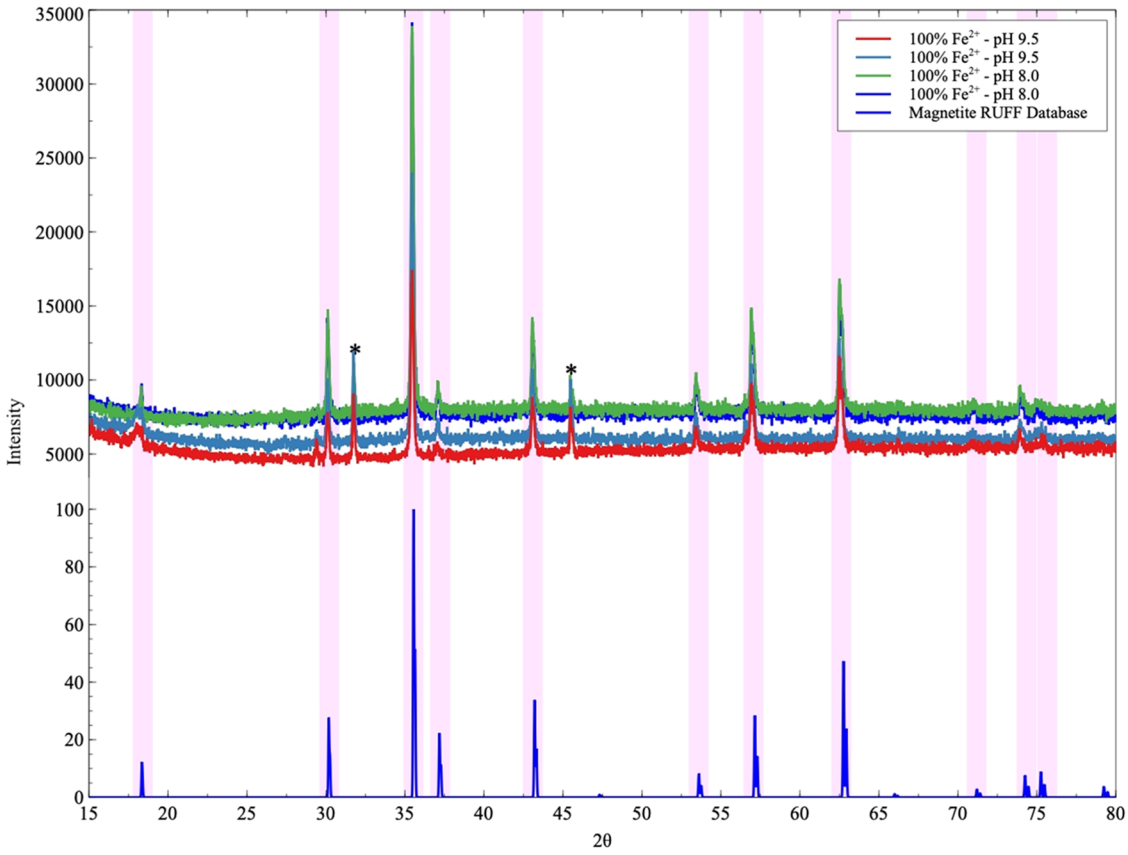

Figure 6. XRD results of experimental repeats of 100% Fe^{2+}–NO_3^- experiments at pH 8.0 and 9.5. Freeze-dried samples of minerals at 1 week compared to magnetite spectra obtained from the RRUFF database (RRUFF ID: R061111.9[22]). The starred peaks (*) correspond to crystalline halite.[23]

found that PO_4^{3-} readily adsorbed onto similar Fe oxyhydroxides and that the degree of adsorption was impacted by pH, coexisting compounds (e.g., amino acids), and mineral type.[33−36] Although we found that NO_3^- did not adsorb onto the Fe minerals, we wanted to see whether it could promote or inhibit HPO_4^{2-} adsorption; simultaneously, we wanted to investigate whether HPO_4^{2-} adsorption onto Fe oxyhydroxides, which may stabilize the mineral and/or shield reaction sites, could affect NO_3^- reduction. All three iron oxidation states (100% Fe^{2+}, 50% Fe^{2+}/50% Fe^{3+}, 100% Fe^{3+}) were tested at pH 9.5 only; we tested 100% Fe^{2+}, which is one condition where we observed NO_3^- reduction the most, and 50% Fe^{2+}/50% Fe^{3+} and 100% Fe^{3+} were the conditions under which we wanted to investigate HPO_4^{2-} adsorption capacity.

100% Fe^{2+} Reactions with Nitrate and Phosphate. In contrast to the NO_3^--only experiments, in nitrate + phosphate experiments at 100% Fe^{2+} and pH 9.5, we observed little to no NO_3^- removal (via adsorption or redox) and no corresponding Fe-mineral oxidation (Figures 7 and 8 and Table S11). Colorimetric results showed that the %Fe^{2+} remained above 97.54% ± 2.02 after 1 week (Figure 8 and Table S2); the Fe precipitates also remained green, indicating that magnetite had not formed (Figure 8). It is thus evident that the addition of the HPO_4^{2-} ion inhibited the NO_3^- −Fe(II)-mineral redox reaction by preventing the transformation of Fe(II)-hydroxides into magnetite. Yet, the mechanism for phosphate to inhibit NO_3^- reduction/Fe oxidation is unclear given that we also observed no retention of the HPO_4^{2-} ion onto the Fe-mineral surface (which would be evidenced by a decrease of HPO_4^{2-}; Figure 7A). The pH of these reactions, like the NO_3^--only experiments, increased from 9.77 ± 0.23 to 11.50 ± 0.41 after 1 week (Table S13). Given that there is no evidence for either NO_3^- or HPO_4^{2-} adsorption or redox reactions, it remains unclear what is facilitating this pH increase. The increase must be related to the presence of NO_3^- given that in control experiments (Fe^{2+} without NO_3^- or HPO_4^{2-} at pH 9.5), only a slight increase in pH from 9.51 at t = 0 to 9.65 at t = 7 days was observed (Table S9).

50% Fe^{2+}/50% Fe^{3+} Reactions with Nitrate and Phosphate. We did not observe any evidence for NO_3^- reduction or Fe oxidation; however, we did observe minor HPO_4^{2-} adsorption in the 50% Fe(II)/50% Fe(III) nitrate + phosphate experiments (Figures 7 and 8); this is again in contrast to our results from the nitrate-only experiments under similar conditions. We also observed a pH increase from 9.5 to ∼11 in the 50% Fe(II) nitrate + phosphate experiments. Similarly, in a previous study, it was observed that nanomagnetite particles experienced less phosphate adsorption with increasing pH; the increased pH was suggested to be a result of OH^- release and phosphate uptake.[37]

100% Fe^{3+} Reactions with Nitrate and Phosphate. Minor HPO_4^{2-} adsorption was observed in the 100% Fe^{3+} nitrate−phosphate experiments at pH 9.5; HPO_4^{2-}adsorption was ∼12% at t = 0 and increased to more than 20% at t = 1 day and ∼28% after t = 1 week (Figure 7A). From this data, it appears that HPO_4^{2-} was adsorbed onto the surface of the ferric (oxy)hydroxides immediately and continued to adsorb more at subsequent time points. Our colorimetric results of 100% Fe^{3+}

https://doi.org/10.1021/acsearthspacechem.3c00218
ACS Earth Space Chem. 2023, 7, 2287−2297

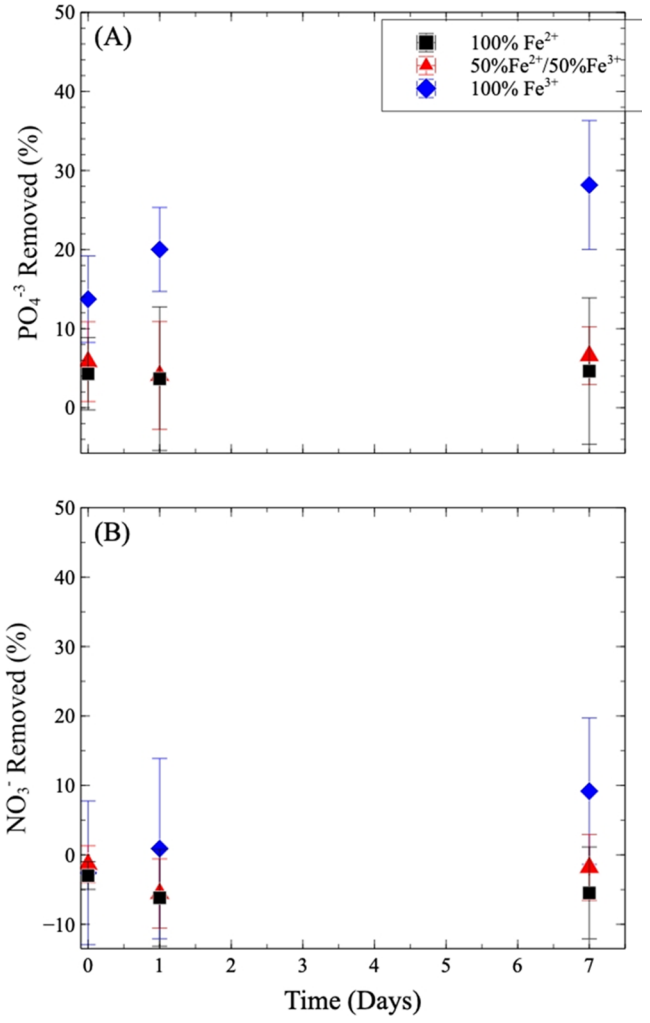

Figure 7. Degree to which (A) HPO_4^{2-} and (B) NO_3^- were removed from solution in experiments containing 50 mM Fe, 25 mM nitrate, and 25 mM phosphate at pH 9.5. Error bars represent the standard deviation of three experimental repeats.

nitrate + phosphate experiments indicate that there were no changes in the Fe redox state, and the precipitate remained as Fe(III) throughout the experiment (Figure 8 and Table S12).

Together, our results show that Fe(II)-driven nitrate oxidation can occur at ambient temperature and alkaline pH, resulting in NH_3/NH_4^+ production in anoxic iron oxyhydroxide mineral systems and conversion to magnetite. Our results taken in context with previous studies indicate that nitrate reduction is highly sensitive to specific chemical conditions such as pH, Fe redox state, concentration ratios of reactants, and the presence of other competing ions. In previous studies, the use of NO_3^- as a mild oxidant has been shown to produce magnetite Fe_3O_4 at elevated temperatures and via oxidation of aqueous Fe(II) bound to Fe minerals, oxidation of zero-valent Fe and green rusts (GR), and other Fe(II) species with added catalysts.[11,12,14,15,25,26,38] Ottley et al., 1997 report an increase in pH will increase reduction rates by Fe(II)-mineral + catalyst reactions, which is in contrast with our results where the rate of reduction was the same despite an increase in the pH.[11] In our redox experiments, the limiting reagent is Fe: oxidation of Fe within metastable Fe-(oxy)-hydroxides results in the formation of magnetite, which is a stable material in wastewater, river water, and in NO_3^--containing solutions.[9,39] Further reduction of NO_3^- in our experiments would likely require additional Fe^{2+} (i.e., the case with surface-bound Fe^{2+} onto magnetite surfaces[25]). In experiments with added Fe^{3+} (50% Fe^{2+}/50% Fe^{3+} and 100% Fe^{3+}), NO_3^- largely remained in solution, which indicates that NO_3^- may be difficult to remove (via adsorption or reduction) in oxidizing systems.

The addition of HPO_4^{2-} into our experiments was to understand if there was any competition between NO_3^- and HPO_4^{2-} on the Fe-mineral surfaces. In a previous work by Flores et al., 2021,[33] we found that 29−45% of phosphate readily adsorbed to ferric and ferrous (oxy)hydroxide precipitates at pH 6.5−8 even in the absence of amino acids that facilitate adsorption.[33] However, in this work, we found that phosphate adsorption was inhibited by the presence of nitrate: no phosphate adsorption was observed with ferrous precipitates at pH 9.5 compared to 45% in ref 33 and only 28% adsorption was observed with ferric precipitates at pH 9.5 (compared to 39% in ref 33). Notably, there was proportionally less iron mineral and thus fewer surface sites available for adsorption in our work that had a lower P:Fe 1:2 compared to the 1:5 ratio used in ref 33. Furthermore, these adsorption reactions were conducted at higher pH (9.5) compared to that in ref 33 where the mineral was precipitated at pH 9, but the adsorption reaction with phosphate was done at pH 6.5. At a lower pH in ref 33, the hematite precipitate (with pzc 6.0−6.5) would be ∼50% positively and ∼50% negatively charged, while phosphate would be mostly in the form of H_2PO_4 ($H_2PO_4 \leftrightarrow HPO_4$; $pK_a \sim 7.2$). H_2PO_4, which is a singly charged anion, can bind to either positive (via the O atom) or negative sites (via the H atoms). However, at pH 9.5 in our work, the hematite mineral is entirely negatively charged, and the phosphate anion would exist as HPO_4, which is a doubly charged anion, and there would be significantly more electrostatic repulsions between the mineral and phosphate ion. Thus, the conditions in our work (even in the absence of nitrate) are less conducive toward phosphate adsorption compared to that in ref 33. Consequently, whether nitrate inhibits phosphate adsorption to ferric oxyhydroxides remains uncertain.

Phosphate is a better nucleophile than NO_3^- (evidenced by phosphate's higher pK_a) and is thus more likely to form bonds at electron-deficient sites on the mineral surface. In our experiments, the mineral reactive sites were likely negatively charged, which would cause electrostatic repulsions from the additional anion species (NO_3^-, Cl^-). The lack of NO_3^- reduction in our 100% Fe(II) nitrate + phosphate experiments can potentially be explained by a mechanism similar to that observed by Etique at al., 2014, where NO_3^- was effectively reduced by green rust ($GR(CO_3^{2-})$) except under conditions where phosphate was introduced into the experiments[38] because phosphate "quasi-saturates" the surface of the green rust and prevented the transition of the green rusts to ferrous hydroxides and magnetite.[38,40] In our experiments, HPO_4^{2-} adsorption may have occurred via weak Lewis acid−base interactions that can inhibit NO_3^- from entering the inner-sphere of the mineral surface; thus, HPO_4^{2-} would have a higher affinity than NO_3^- to the mineral surface, which would allow HPO_4^{2-} to remain in the inner-sphere region of the mineral matrix, while NO_3^- would remain inert at the outer-sphere region. The outer and inner-sphere mechanisms are explained by the effects of ionic strength that render the molecules inefficient at adsorbing onto the mineral surface in the presence of other anions.[41] In a Mg−Mn layered double

https://doi.org/10.1021/acsearthspacechem.3c00218
ACS Earth Space Chem. 2023, 7, 2287−2297

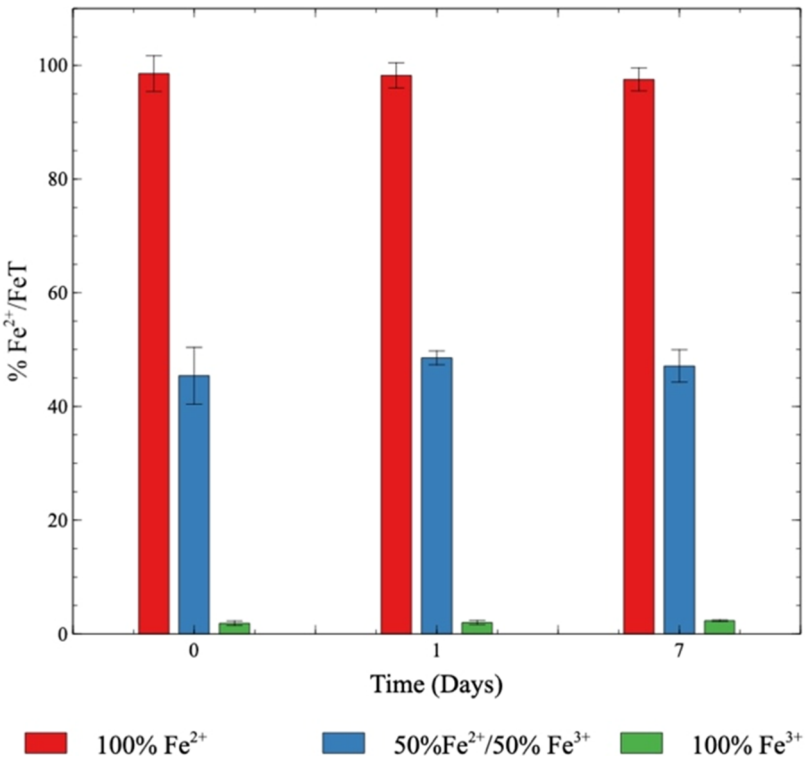

Figure 8. Percent Fe^{2+} for experiments with 50 mM Fe, 25 mM NO_3^-, and 25 mM HPO_4^{2-}. Error bars represent the standard deviation of three experimental repeats. Note that there was no significant oxidation of Fe(II) in any of the experiments containing HPO_4^{2-}.

hydroxide experiment, for example, the adsorption of phosphate (using seawater containing phosphate) occurred via electrostatic forces and had a maximum adsorption capacity near pH 8.5, which decreased with increasing pH.[42] Zhang et al., 2019 performed similar experiments with a similarly prepared ferric iron precipitate and determined that there was significantly lower phosphate adsorption at pH ≥ 9.0; however, they did find a correlation between higher salinity (NaCl) content and higher PO_4^{3-} adsorption on minerals at alkaline pH.[43] They also evaluated how NaCl can form sodium-phosphate species (e.g., $NaHPO_4^-$, Na2HPO_4 (aq)) to provide a positively charged ionic complex to the negatively charged mineral surface; likewise, they suggested that Na^+ can decrease electrostatic repulsions in the system.[43] In our experiments, Na^+ is abundant since we used $NaNO_3$, $NaPO_4^3$, and NaOH salts. The values we report here agree with those found by Zhang et al., 2019, assuming Na^+ facilitated phosphate adsorption onto the ferric (oxy)hydroxide precipitates.

In an environmental science context, both NO_3^- and HPO_4^{2-} would be mobile and can potentially contaminate surface water and groundwater. Additionally, NO_3^- reduced to NH_3/NH_4^+ poses additional N contamination problems, as NH_3/NH_4^+ can exacerbate eutrophic conditions in surface waters. Furthermore, variations in these and other conditions likely to be encountered in the environment should be considered as significant drivers affecting the likelihood of NO_3^- reduction that would occur in natural systems and/or should be considered as parameters that can be controlled to predict nitrate reduction rates in a water treatment context.

■ ASSOCIATED CONTENT

Supporting Information

The Supporting Information is available free of charge at https://pubs.acs.org/doi/10.1021/acsearthspacechem.3c00218.

Additional details on experimental conditions; ion chromatography data, spectrophotometry calibration curves; colorimetry data; and pH measurements (PDF)

■ AUTHOR INFORMATION

Corresponding Authors

Eduardo Martinez − *NASA Jet Propulsion Laboratory, California Institute of Technology, Pasadena, California 91109, United States; Department of Civil Engineering, California State University Los Angeles, Los Angeles, California 90032, United States;* orcid.org/0009-0007-4222-0334; Email: meduardoce@gmail.com

Laura M. Barge − *NASA Jet Propulsion Laboratory, California Institute of Technology, Pasadena, California 91109, United States;* orcid.org/0000-0002-2187-540X; Email: laura.m.barge@jpl.nasa.gov

Authors

Laura E. Rodriguez − *NASA Jet Propulsion Laboratory, California Institute of Technology, Pasadena, California 91109, United States; Lunar and Planetary Institute, Universities Space Research Association, Houston, Texas 77058, United States*

Rachel Y. Sheppard − *NASA Jet Propulsion Laboratory, California Institute of Technology, Pasadena, California 91109, United States*

https://doi.org/10.1021/acsearthspacechem.3c00218
ACS Earth Space Chem. 2023, 7, 2287−2297

Yi Zhang − *Linde Laboratories, California Institute of Technology, Pasadena, California 91125, United States;* orcid.org/0000-0002-9062-5201
Clément A. Cid − *Linde Laboratories, California Institute of Technology, Pasadena, California 91125, United States*
Arezoo Khodayari − *Department of Civil Engineering, California State University Los Angeles, Los Angeles, California 90032, United States*

Complete contact information is available at: https://pubs.acs.org/10.1021/acsearthspacechem.3c00218

Author Contributions

The manuscript was written through contributions of all authors. All authors have given approval to the final version of the manuscript.

Notes

The authors declare no competing financial interest.

■ ACKNOWLEDGMENTS

E.M., L.E.R., and L.M.B. were supported by the NASA Habitable Worlds program "Phosphorus Redox Chemistry on Icy and Rocky Planets". R.Y.S. was supported by a JPL Strategic Research & Technology Development award. This research was carried out at the Jet Propulsion Laboratory, California Institute of Technology, under a contract with the National Aeronautics and Space Administration (80NM0018D0004).

■ REFERENCES

(1) Summers, D. P.; Chang, S. Prebiotic ammonia from reduction of nitrite by iron (II) on the early Earth. *Nature* **1993**, *365* (6447), 630−633.
(2) Thayalakumaran, T.; Bristow, K. L.; Charlesworth, P. B.; Fass, T. Geochemical conditions in groundwater systems: Implications for the attenuation of agricultural nitrate. *Agric. Water Manage.* **2008**, *95* (2), 103−115.
(3) Liu, H.; Chen, Z.; Guan, Y.; Xu, S. Role and application of iron in water treatment for nitrogen removal: a review. *Chemosphere* **2018**, *204*, 51−62.
(4) Borggaard, O. K. The influence of iron oxides on phosphate adsorption by soil. *J. Soil Sci.* **1983**, *34* (2), 333−341.
(5) Doane, T. A. The abiotic nitrogen cycle. *ACS Earth Space Chem.* **2017**, *1* (7), 411−421.
(6) Mejia, J.; Roden, E. E.; Ginder-Vogel, M. Influence of oxygen and nitrate on Fe (hydr) oxide mineral transformation and soil microbial communities during redox cycling. *Environ. Sci. Technol.* **2016**, *50* (7), 3580−3588.
(7) Usman, M.; Byrne, J. M.; Chaudhary, A.; Orsetti, S.; Hanna, K.; Ruby, C.; Kappler, A.; Haderlein, S. B. Magnetite and green rust: synthesis, properties, and environmental applications of mixed-valent iron minerals. *Chem. Rev.* **2018**, *118* (7), 3251−3304.
(8) Pincus, L. N.; Rudel, H. E.; Petrović, P. V.; Gupta, S.; Westerhoff, P.; Muhich, C. L.; Zimmerman, J. B. Exploring the mechanisms of selectivity for environmentally significant oxo-anion removal during water treatment: a review of common competing oxo-anions and tools for quantifying selective adsorption. *Environ. Sci. Technol.* **2020**, *54* (16), 9769−9790.
(9) Dhakal, P.; Matocha, C. J.; Huggins, F. E.; Vandiviere, M. M. Nitrite reactivity with magnetite. *Environ. Sci. Technol.* **2013**, *47* (12), 6206−6213.
(10) Mürbe, J.; Rechtenbach, A.; Töpfer, J. Synthesis and physical characterization of magnetite nanoparticles for biomedical applications. *Mater. Chem. Phys.* **2008**, *110* (2−3), 426−433.
(11) Ottley, C. J.; Davison, W.; Edmunds, W. M. Chemical catalysis of nitrate reduction by iron (II). *Geochim. Cosmochim. Acta* **1997**, *61*, 1819−1828.
(12) Buresh, R. J.; Moraghan, J. T. Chemical reduction of nitrate by ferrous iron (Vol. 5, No. 3, pp. 320−325). *J. Environ. Qual.* **1976**, *5* (3), 320−325.
(13) Song, H.; Jeon, B. H.; Chon, C. M.; Kim, Y.; Nam, I. H.; Schwartz, F. W.; Cho, D. W. The effect of granular ferric hydroxide amendment on the reduction of nitrate in groundwater by zero-valent iron. *Chemosphere* **2013**, *93* (11), 2767−2773.
(14) Vereda, F.; De Vicente, J.; Hidalgo-Alvarez, R. Oxidation of ferrous hydroxides with nitrate: A versatile method for the preparation of magnetic colloidal particles. *J. Colloid Interface Sci.* **2013**, *392*, 50−56.
(15) Hansen, H. C. B.; Koch, C. B.; Nancke-Krogh, H.; Borggaard, O. K.; Sørensen, J. Abiotic nitrate reduction to ammonium: key role of green rust. *Environ. Sci. Technol.* **1996**, *30* (6), 2053−2056.
(16) Acelas, N. Y.; Hadad, C.; Restrepo, A.; Ibarguen, C.; Flórez, E. Adsorption of nitrate and bicarbonate on Fe-(Hydr) oxide. *Inorg. Chem.* **2017**, *56* (9), 5455−5464.
(17) Choi, J.; Suryanto, B. H.; Wang, D.; Du, H. L.; Hodgetts, R. Y.; Ferrero Vallana, F. M.; MacFarlane, D. R.; Simonov, A. N. Identification and elimination of false positives in electrochemical nitrogen reduction studies. *Nat. Commun.* **2020**, *11* (1), No. 5546, DOI: 10.1038/s41467-020-19130-z.
(18) Barge, L. M.; Flores, E.; Weber, J. M.; Fraeman, A. A.; Yung, Y. L.; VanderVelde, D.; Martinez, E.; Castonguay, A.; Billings, K.; Baum, M. M. Prebiotic reactions in a Mars analog iron mineral system: Effects of nitrate, nitrite, and ammonia on amino acid formation. *Geochim. Cosmochim. Acta* **2022**, *336*, 469−479.
(19) Muramatsu, K. Direct colorimetric method for the determination of free ammonia in blood. *Agric. Biol. Chem.* **1967**, *31* (3), 301−308.
(20) Aguirre, V. P.; Jocic, S.; Webster, P.; Buser, C.; Moss, J. A.; Barge, L. M.; Tang, Y.; Guo, Y.; Baum, M. M. Synthesis and characterization of mixed-valent iron layered double hydroxides ("green rust"). *ACS Earth Space Chem.* **2021**, *5* (1), 40−54.
(21) Ficai, D.; Ficai, A.; Vasile, B. S.; Ficai, M.; Oprea, O.; Guran, C.; Andronescu, E. Synthesis of rod-like magnetite by using low magnetic field. *Digest J. Nanomater. Biostructures* **2011**, *6*, 943−951.
(22) Lafuente, B.; Downs, R. T.; Yang, H.; Stone, N. The power of databases: the RRUFF project. In *Highlights in Mineralogical Crystallography*; Armbruster, T.; Danisi, R. M., Eds.; W. De Gruyter: Berlin, Germany, 2015.
(23) Borrego-Sánchez, A.; Gutiérrez-Ariza, C.; Sainz-Díaz, C. I.; Cartwright, J. H. The Effect of the Presence of Amino Acids on the Precipitation of Inorganic Chemical-Garden Membranes: Biomineralization at the Origin of Life. *Langmuir* **2022**, *38*, 10538−10547, DOI: 10.1021/acs.langmuir.2c01345.
(24) Jolivet, J. P.; Chanéac, C.; Tronc, E. Iron oxide chemistry. From molecular clusters to extended solid networks. *Chem. Commun.* **2004**, No. 5, 481−483, DOI: 10.1039/B304532N.
(25) Huang, Y. H.; Zhang, T. C. Nitrate Reduction by Surface-Bound Fe(II) on Solid Surfaces at Near-Neutral pH and Ambient Temperature. *J. Environ. Eng.* **2016**, No. 1−7, No. 04016053, DOI: 10.1061/(ASCE)EE.1943-7870.0001130.
(26) Tennakone, K.; Bandara, J. M. S.; Thaminimulla, C. T. K.; Jayatilake, W. D. W.; Ketipearachchi, U. S.; Ileperuma, O. A.; Priyadarshana, M. K. A. Photoreduction of dinitrogen to ammonia by ultrafine particles of iron hydroxide oxide (Fe(O)OH) formed by photohydrolysis of iron (II) bicarbonate. *Langmuir* **1991**, *7* (10), 2166−2168.
(27) Génin, J. M. R.; Ruby, C.; Géhin, A.; Refait, P. Synthesis of green rusts by oxidation of Fe (OH) 2, their products of oxidation and reduction of ferric oxyhydroxides; Eh−pH Pourbaix diagrams. *C. R. Geosci.* **2006**, *338* (6−7), 433−446.
(28) Youngran, J.; Maohong, F. A. N.; Van Leeuwen, J.; Belczyk, J. F. Effect of competing solutes on arsenic (V) adsorption using iron

and aluminum oxides. *J. Environ. Sci.* **2007**, *19* (8), 910−919, DOI: 10.1016/s1001-0742(07)60151-x.
(29) Parfitt, R. L.; Russell, J. D. Adsorption on hydrous oxides. IV. Mechanisms of adsorption of various ions on goethite. *J. Soil Sci.* **1977**, *28* (2), 297−305.
(30) Chitrakar, R.; Tezuka, S.; Sonoda, A.; Sakane, K.; Ooi, K.; Hirotsu, T. Phosphate adsorption on synthetic goethite and akaganeite. *J. Colloid Interface Sci.* **2006**, *298* (2), 602−608.
(31) Lützenkirchen, J.; Heberling, F.; Supljika, F.; Preocanin, T.; Kallay, N.; Johann, F.; Weisser, L.; Eng, P. J. Structure−charge relationship−the case of hematite (001). *Faraday Discuss.* **2015**, *180*, 55−79.
(32) Wang, Y.; Persson, P.; Michel, F. M.; Brown, G. E., Jr Comparison of isoelectric points of single-crystal and polycrystalline α-Al2O3 and α-Fe2O3 surfaces. *Am. Mineral.* **2016**, *101* (10), 2248−2259.
(33) Flores, E.; Martinez, E.; Rodriguez, L. E.; Weber, J. M.; Khodayari, A.; VanderVelde, D. G.; Barge, L. M. Effects of amino acids on phosphate adsorption onto iron (oxy) hydroxide minerals under early earth conditions. *ACS Earth Space Chem.* **2021**, *5* (5), 1048−1057.
(34) Kim, J.; Li, W.; Philips, B. L.; Grey, C. P. Phosphate adsorption on the iron oxyhydroxides goethite (α-FeOOH), akaganeite (β-FeOOH), and lepidocrocite (γ-FeOOH): a 31 P NMR study. *Energy Environ. Sci.* **2011**, *4* (10), 4298−4305.
(35) Colombo, C.; Barrón, V.; Torrent, J. Phosphate adsorption and desorption in relation to morphology and crystal properties of synthetic hematites. *Geochim. Cosmochim. Acta* **1994**, *58* (4), 1261−1269.
(36) Elzinga, E. J.; Sparks, D. L. Phosphate adsorption onto hematite: An in situ ATR-FTIR investigation of the effects of pH and loading level on the mode of phosphate surface complexation. *J. Colloid Interface Sci.* **2007**, *308* (1), 53−70.
(37) Daou, T. J.; Begin-Colin, S.; Greneche, J. M.; Thomas, F.; Derory, A.; Bernhardt, P.; Legaré, P.; Pourroy, G. Phosphate adsorption properties of magnetite-based nanoparticles. *Chem. Mater.* **2007**, *19* (18), 4494−4505.
(38) Etique, M.; Zegeye, A.; Grégoire, B.; Carteret, C.; Ruby, C. Nitrate reduction by mixed iron (II-III) hydroxycarbonate green rust in the presence of phosphate anions: The key parameters influencing the ammonium selectivity. *Water Res.* **2014**, *62*, 29−39.
(39) Klekotka, U.; Zambrzycka-Szelewa, E.; Satuła, D.; Kalska-Szostko, B. Stability studies of magnetite nanoparticles in environmental solutions. *Materials* **2021**, *14* (17), 5069.
(40) Bocher, F.; Géhin, A.; Ruby, C.; Ghanbaja, J.; Abdelmoula, M.; Génin, J. M. R. Coprecipitation of Fe (II−III) hydroxycarbonate green rust stabilised by phosphate adsorption. *Solid State Sci.* **2004**, *6* (1), 117−124.
(41) Almasri, D. A.; Saleh, N. B.; Atieh, M. A.; McKay, G.; Ahzi, S. Adsorption of phosphate on iron oxide doped halloysite nanotubes. *Sci. Rep.* **2019**, *9* (1), No. 3232, DOI: 10.1038/s41598-019-39035-2.
(42) Chitrakar, R.; Tezuka, S.; Sonoda, A.; Sakane, K.; Ooi, K.; Hirotsu, T. Adsorption of phosphate from seawater on calcined MgMn-layered double hydroxides. *J. Colloid Interface Sci.* **2005**, *290* (1), 45−51.
(43) Zhang, H.; Elskens, M.; Chen, G.; Chou, L. Phosphate adsorption on hydrous ferric oxide (HFO) at different salinities and pHs. *Chemosphere* **2019**, *225*, 352−359.

https://doi.org/10.1021/acsearthspacechem.3c00218
ACS Earth Space Chem. 2023, 7, 2287−2297